Abstracta

Ano XXVII - N. 04

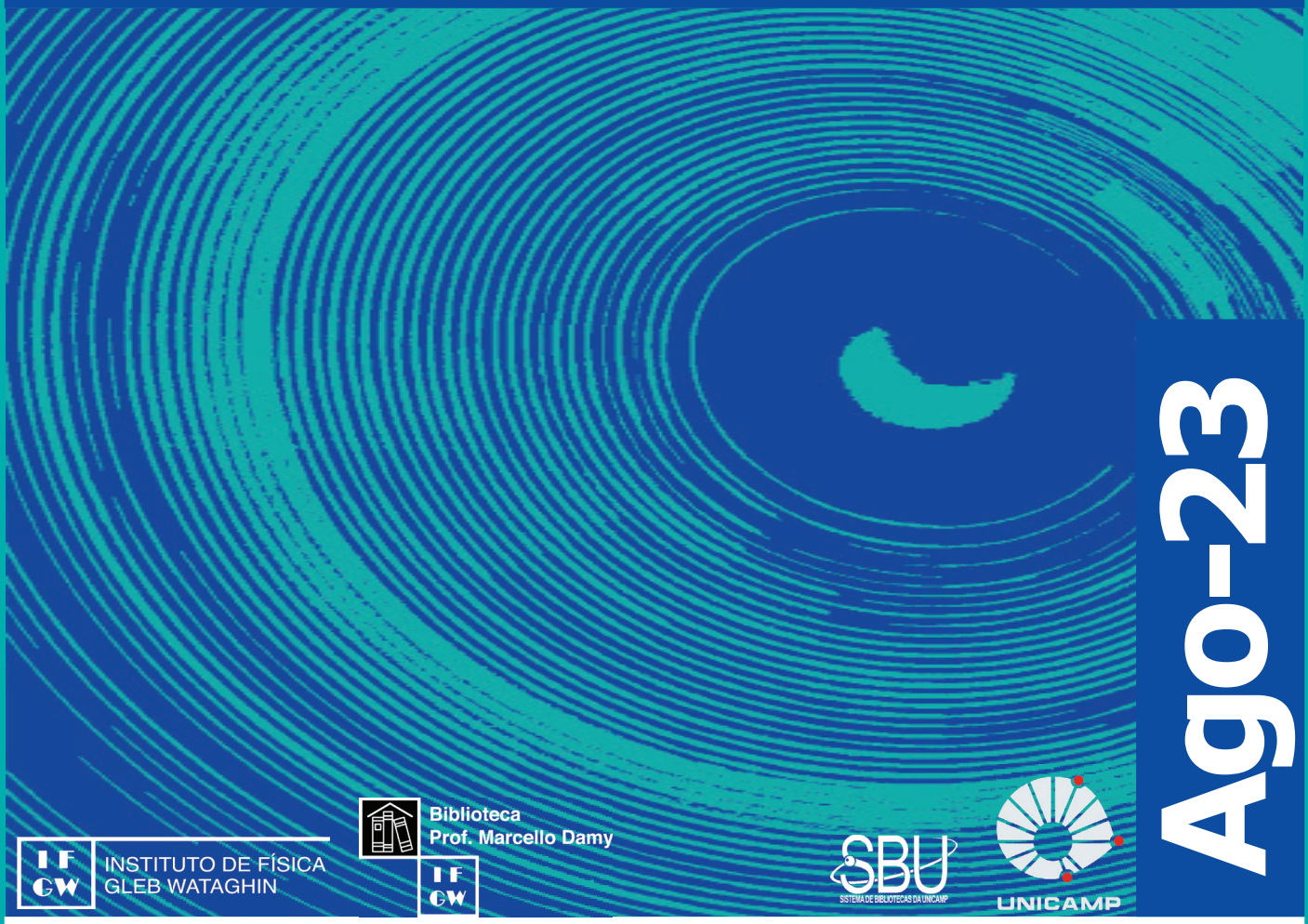

Artigos publicados - P103-2023 à P153-2023

Defesas de Dissertações do IFGW - D011-2023 à D017-2023

Defesas de Teses do IFGW - T009-2023 à T10-2023

Defesas de Dissertações e Teses do PECIM - Pe002-2023

Artigos publicados

[P103-2023] "1337 nm Emission of a Nd3+-Doped TZA Glass Random Laser"

Dipold, J.; Bordon, C. D. S.; Magalhaes, E. S.; Kassab, L. R. P.; **Jimenez-Villar, E.***; Wetter, N. U.

Random lasers have been studied using many materials, but only a couple have used glass matrices. Here, we present a study of zinc tellurite and aluminum oxide doped with different percentages of neodymium oxide (4 wt.%, 8 wt.%, and 16 wt.%) and demonstrate for the first time random laser action at 1337 nm. Laser emission was verified and the laser pulse's rise time and input-output power slope were obtained. A cavity composed of the sample's pump surface and an effective mirror formed by a second, parallel layer at the gain-loss boundary was probably the main lasing mechanism of this random laser system. The reason for the absence of emission at 1064 nm is thought to be a measured temperature rise in the samples' active volume.

NANOMATERIALS 13[13], 1972, 2023. DOI: 10.3390/nano13131972

[P104-2023] "A Catalog of the Highest-energy Cosmic Rays Recorded during Phase I of Operation of the Pierre Auger Observatory"

Halim, A. A.; Abreu, P.; **Arbeletche, L. B.*; Chinellato, J. A.*; Franco, D. de O.*; Dobrigkeit, C.*; Fauth, A. C.*; Payeras, A. M.*; Muller, M. A.***; et al. Pierre Auger Collaboration

A catalog containing details of the highest-energy cosmic rays recorded through the detection of extensive air showers at the Pierre Auger Observatory is presented with the aim of opening the data to detailed examination. Descriptions of the 100 showers created by the highest-energy particles recorded between 2004 January 1 and 2020 December 31 are given for cosmic rays that have energies in the range 78-166 EeV. Details are also given on a further nine very energetic events that have been used in the calibration procedure adopted to determine the energy of each primary. A sky plot of the arrival directions of the most energetic particles is shown. No interpretations of the data are offered.

ASTROPHYSICAL JOURNAL SUPPLEMENT SERIES 264[2], 50, 2023. DOI: 10.3847/1538-4365/aca537

[P105-2023] "Batch and continuous adsorption of Cd(II) and Pb(II) on polycarboxylated sugarcane bagasse"

Elias, M. M. C.; Soares, L. C.; Maia, L. C.; Taylor, J. G.; Adarme, O. F. H.; Ferreira, G. M. D.; Azevedo, E. R. de; **Siervo, A. de*;** Silva, L. H. M. da; Gurgel, L. V. A.

A bioadsorbent composed of polycarboxylated sugarcane bagasse (PSB) was prepared in a one-step reaction by the esterification of sugarcane bagasse hydroxyl groups with butane-1,2,3,4--tetracarboxylic dianhydride. 13C SS NMR measurements showed that 0.3 butane-1,2,3,4-tetracarboxylic acid units were grafted per cellobiose unit. PSB was used in the batch adsorption of Cd(II) and Pb(II) from mono-, bi-, and multicomponent aqueous so-lutions. For upscaling of the technology aiming at practical applications, evaluation was made of 4 cycles of continuous adsorption of Cd(II) and Pb(II) on PSB in a fixed-bed column. The maximum adsorption capacities for Cd(II) and Pb(II) on PSB in batch and continuous modes were 0.55 and 1.164 mmol g- 1 (62 and 241.2 mg g-1), and 0.58 and 0.71 mmol g- 1 (65 and 153 mg g-1), respectively. The standard adsorption enthalpy change (& UDelta;adsH degrees) values for Cd(II) and Pb(II) were 8.6 & PLUSMN; 0.5 and -0.28 & PLUSMN; 0.03 kJ mol-1, respectively. The interactions involved in the adsorption of Cd(II) and Pb(II) on PSB were investigated. Multicomponent studies showed that Pb (II) and Cd(II) acted to suppress the adsorption of each other. In the presence of Cu(II) and Zn(II), the adsorption capacity followed the order: Pb(II) > Cu(II) > Cd(II) > Zn(II). Batch and continuous adsorption-desorption studies showed that PSB could be reused in at least 4 successive cycles, with desorption efficiencies of 88-100 %, which is essential for minimizing waste generation and reducing process costs.

JOURNAL OF WATER PROCESS ENGINEERING 54, 103947, 2023. DOI: 10.1016/j.jwpe.2023.103947

[P106-2023] "Constraining hadronization mechanisms with A(c)(+) /D-0 production ratios in Pb-Pb collisions at root(NN)--N-s=5.02 TeV"

Acharya, S.; Adamova, D.; **Chinellato, D. D.*; Guardiano, G. G.*; Jahnke, C.*; Takahashi, J.***; et al. ALICE Collaboration

The production of prompt A+c baryons at midrapidity (|y| < 0.5) was measured in central (0-10%) and mid-central (30-50%) Pb-Pb collisions at the center-of-mass energy per nucleon--nucleon pair root sNN = 5.02 TeV with the ALICE detector. The results are more precise, more differential in centrality, and reach much lower transverse momentum (pT =1 GeV/c) with respect to previous measurements performed by the ALICE, STAR, and CMS Collaborations in nucleus-nucleus collisions, allowing for an extrapolation down to pT = 0. The pT--differential A+c /D0 ratio is enhanced with respect to the pp measurement for 4 < pT < 8 GeV/c by 3.7 standard deviations (cr), while the pT-integrated ratios are compatible within 1cr. The observed trend is similar to that observed in the strange sector for the A/K0S ratio. Model calculations including coalescence or statistical hadronization for charm-hadron formation are compared with the data.(c) 2023 European Organization for Nuclear Research. Published by Elsevier B.V. This is an open access article under the CC BY license (http://creativecommons .org /licenses /by /4 .0/). Funded by SCOAP3.

PHYSICS LETTERS B 839, 137796, 2023. DOI: 10.1016/j.physletb.2023.137796

[P107-2023] "Correlation versus hybridization gap in CaMn-2Bi2"

Lane, C.; **Piva, M. M.***; Rosa, P. F. S.; Zhu, J. X.

We study the interplay between electronic correlations and hybridization in the low-energy electronic structure of CaMn2Bi2, a candidate hybridization-gap semiconductor. By employing a DFT+U approach we find both the antiferromagnetic Neel order and band gap in good agreement with the corresponding experimental values. Under hydrostatic pressure, we find a crossover from hybridization gap to charge-transfer insulting physics due to the delicate balance of hybridization and correlations. Increasing the pressure above P-c = 4 GPa we find a simultaneous pressure-induced volume collapse, plane-to-chain, insulator to metal transition. Finally, we have also analyzed the topology in the antiferromagnetic CaMn2Bi2 for all pressures studied.

SCIENTIFIC REPORTS 13[1], 9371, 2023. DOI: 10.1038/s41598-023-35812-2

[P108-2023] "Cosmological implications of photon-flux upper limits at ultrahigh energies in scenarios of Planckian--interacting massive particles for dark matter"

Abreu, P.; Aglietta, M.; **Arbeletche, L. B.*; Chinellato, J. A.*; Franco, D. de O.*; Dobrigkeit, C.*; Fauth, A. C.*; Payeras, A. M.*; Muller, M. A.***; et al. Pierre Auger Collaboration

Using the data of the Pierre Auger Observatory, we report on a search for signatures that would be suggestive of super-heavy particles decaying in the Galactic halo. From the lack of signal, we present upper limits for different energy thresholds above greater than or similar to 108 GeV on the secondary by-product fluxes expected from the decay of the particles. Assuming that the energy density of these super-heavy particles matches that of dark matter observed today, we translate the upper bounds on the particle fluxes into tight constraints on the couplings governing the decay process as a function of the particle mass. Instantons, which are nonperturbative solutions to Yang-Mills equations, can give rise to decay channels otherwise forbidden and transform stable particles into metastable ones. Assuming such instanton-induced decay processes, we derive a bound on the reduced coupling constant of gauge interactions in the dark sector: alpha X < 0.09, for 109 < MX=GeV < 1019. Conversely, we obtain that, for instance, a reduced coupling constant alpha X 1/4 0.09 excludes masses MX greater than or similar to 3 x 1013 GeV. In the context of dark matter production from gravitational interactions alone during the reheating epoch, we derive constraints on the parameter space that involves, in addition to MX and alpha X, the Hubble rate at the end of inflation, the reheating efficiency, and the nonminimal coupling of the Higgs with curvature.

PHYSICAL REVIEW D 107[4], 042002, 2023. DOI: 10.1103/PhysRevD.107.042002

[P109-2023] "Dielectron production at midrapidity at low transverse momentum in peripheral and semi-peripheral Pb--Pb collisions at root s(NN)=5.02 TeV"

Acharya, S.; Adamova, D.; **Chinellato, D. D.*; Guardiano, G. G.*; Jahnke, C.*; Takahashi, J.***; et al. Alice Collaboration

The first measurement of the e(+)e(-) pair production at low lepton pair transverse momentum (p(T,ee)) and low invariant mass (m(ee)) in non-central Pb-Pb collisions at root s(NN) = 5.02TeV at the LHC is presented. The dielectron production is studied with the ALICE detector at midrapidity (vertical bar eta(e)vertical bar < 0.8) as a function of invariant mass (0.4 <= m(ee) < 2.7 GeV/c(2)) in the 50-70% and 70-90% centrality classes for p(T,ee) < 0.1 GeV/c, and as a function of p(T,ee) in three m(ee) intervals in the most peripheral Pb-Pb collisions. Below a p(T,ee) of 0.1 GeV/c, a clear excess of e(+) e(-) pairs is found compared to the expectations from known hadronic sources and predictions of thermal radiation from the medium. The m(ee) excess spectra are reproduced, within uncertainties, by different predictions of the photon-photon production of dielectrons, where the photons originate from the extremely strong electromagnetic fields generated by the highly Lorentz-contracted Pb nuclei. Lowest-order quantum electrodynamic (QED) calculations, as well as a model that takes into account the impact-parameter dependence of the average transverse momentum of the photons, also provide a good description of the p(T,ee) spectra. The measured root < p(T,ee)(2)> of the excess p(T,ee) spectrum in peripheral Pb-Pb collisions is found to be comparable to the values observed previously at RHIC in a similar phase-space region.

JOURNAL OF HIGH ENERGY PHYSICS [6], 024, 2023. DOI: 10.1007/JHEP06(2023)024

[P110-2023] "Effect of Host-Switching on the Ecological and Evolutionary Patterns of Parasites"

D'Bastiani, E.; **Princepe, D.*; Marquitti, F. M. D.***; Boeger, W. A.; Campiao, K. M.; Araujo, S. B. L.

Speciation via host-switching is a macroevolutionary process that emerges from a microevolutionary dynamic where individual parasites switch hosts, establish a new association, and reduce reproductive contact with the original parasite lineage. Phylogenetic distance and geographic distribution of the hosts have been shown to be determinants of the capacity and opportunity of the parasite to change hosts. Although speciation via host-switching has been reported in many host-parasite systems, its dynamic on the individual, population and community levels is poorly understood. Here we propose a theoretical model to simulate parasite evolution considering host-switching events on the microevolutionary scale, taking into account the macroevolutionary history of the hosts, to evaluate how host--switching can affect ecological and evolutionary patterns of parasites in empirical communities at regional and local scales. In the model, parasite individuals can switch hosts under variable intensity and have their evolution driven by mutation and genetic drift. Mating is sexual and only individuals that are sufficiently similar can produce offspring. We assumed that parasite evolution occurs at the same evolutionary time scale as their hosts, and that the intensity of host-switching decreases as the host species differentiate. Ecological and evolutionary patterns were characterized by the turnover of parasite species among host species, and parasite evolutionary tree imbalance respectively. We found a range of host-switching intensity that reproduces ecological and evolutionary patterns observed in empirical communities. Our results showed that turnover decreased as host-switching intensity increased, with low variation among the model replications. On the other hand, tree imbalance showed wide variation and non-monotonic tendency. We concluded that tree imbalance was sensitive to stochastic events, whereas turnover may be a good indicator of host-switching. We found that local communities corresponded to higher host--switching intensity when compared to regional communities, highlighting that spatial scale is a limitation for host-switching. [Dispersal of parasites, opportunity and capacity of interaction, phylogenetic conservatism, and community structure.]

SYSTEMATIC BIOLOGY, 2023. DOI: 10.1093/sysbio/syad022
Primeira data de acesso: APR 2023

[P111-2023] "Elastocaloric Effect in Graphene Kirigami"

Ribeiro Junior, L. A. R.; Pereira Junior, M. L. L.; **Fonseca, A. F.***

Kirigami, a traditional Japanese art of paper cutting,has recentlybeen explored for its elastocaloric effect (ECE) in kirigami-basedmaterials (KMs), where an applied strain induces temperature changes.Importantly, the feasibility of a nanoscale graphene kirigami monolayerwas experimentally demonstrated. Here, we investigate the ECE in GKrepresenting the thinnest possible KM to better understand this phenomenon. Through molecular dynamics simulations, we analyze the temperaturechange and coefficient of performance (COP) of GK. Our findings revealthat while GKs lack the intricate temperature changes observed inmacroscopic KMs, they exhibit a substantial temperature change ofapproximately 9.32 K (23 times higher than that of macroscopic KMs,which is about 0.4 K) for heating and -3.50 K for cooling.Furthermore, they demonstrate reasonable COP values of approximately1.57 and 0.62, respectively. It is noteworthy that the one-atom-thickgraphene configuration prevents the occurrence of the complex temperaturedistribution observed in macroscopic KMs.

NANO LETTERS, 2023. DOI: 10.1021/acs.nanolett.3c02260
Primeira data de acesso: JUL 2023

[P112-2023] "Enhanced Light Scattering Using a Two-Dimensional Quasicrystal-Decorated 3D-Printed Nature-Inspired Bio-photonic Architecture"

Kumbhakar, P.; Pramanik, A.; Mishra, S. S.; **Tromer, R.***; Biswas, K.; Dasgupta, A.; **Galvao, D. S.***; Tiwary, C. S.

A numberof strategies have been exploited so far to trap photonsinside living cells to obtain high-contrast imaging.

Also, launchinglight inside biological materials is technically challenging. Usingphoton confinement in a three-dimensional (3D)-printed biomimeticarchitecture in the presence of a localized surface plasmon resonance(LSPR) promoter can overcome some of these issues. This work comparesoptical confinement in natural and 3D-printed photonic architectures,namely, fish scale, in the presence of atomically thin Al70Co10Fe5Ni10Cu5 quasicrystals(QCs). Due to their wideband LSPR response, the QCs work as photonscattering hotspots. The architecture acts as an additive source ofexcitation for the two-dimensional (2D) QCs via total internal reflection(TIR). The computational analysis describes the surface plasmon--basedscattering property of 2D QCs. The 3D-printed fish scale'simage contrast with the 2D Al70Co10Fe5Ni10Cu5 QC has been compared with other 2Dmaterials (graphene, h-BN, and MoS2) and outperforms them.The present study conceptually presents a new approach for obtaininghigh-quality imaging of biological imaging, even using high-energyphotons.

JOURNAL OF PHYSICAL CHEMISTRY C 127[20], 9779-9786, 2023. DOI: 10.1021/acs.jpcc.3c00513

[P113-2023] "Estimating the impact of implementation and timing of the COVID-19 vaccination programme in Brazil: a counterfactual"

Ferreira, L. S.; **Marquitti, F. M. D.***; Silva, R. L. P. da; Borges, M. E.; Gomes, M. F. da C.; Cruz, O. G.; Kraenkel, R. A.; Coutinho, R. M.; Prado, P. I.; Bastos, L. S.

Background Vaccines developed between 2020 and 2021 against the SARS-CoV-2 virus were designed to diminish the severity and prevent deaths due to COVID-19. However, estimates of the effectiveness of vaccination campaigns in achieving these goals remain a methodological challenge. In this work, we developed a Bayesian statistical model to estimate the number of deaths and hospitalisations averted by vaccination of older adults (above 60 years old) in Brazil.Methods We fit a linear model to predict the number of deaths and hospitalisations of older adults as a function of vaccination coverage in this group and casualties in younger adults. We used this model in a counterfactual analysis, simulating alternative scenarios without vaccination or with faster vaccination roll-out. We estimated the direct effects of COVID-19 vaccination by computing the difference between hypothetical and realised scenarios. Findings We estimated that more than 165,000 individuals above 60 years of age were not hospitalised due to COVID-19 in the first seven months of the vaccination campaign. An additional contingent of 104,000 hospitalisations could have been averted if vaccination had started earlier. We also estimated that more than 58 thousand lives were saved by vaccinations in the period analysed for the same age group and that an additional 47 thousand lives could have been saved had the Brazilian government started the vaccination programme earlier.Interpretation Our estimates provided a lower bound for vaccination impacts in Brazil, demonstrating the importance of preventing the suffering and loss of older Brazilian adults. Once vaccines were approved, an early vaccination roll-out could have saved many more lives, especially when facing a pandemic.Funding The Coordenacao de Aperfeicoamento de Pessoal de Nivel Superior-Brazil (Finance Code 001 to F.M.D.M. and L.S.F.), Conselho Nacional de Desenvolvimento Cientifico e Tecnologico - Brazil (grant number: 315854/2020-0 to M.E.B., 141698/2018-7 to R.L.P.d.S., 313055/2020-3 to P.I.P., 311832/2017-2 to R.A.K.), Fundacao de Amparo a Pesquisa do Estado de Sao Paulo - Brazil (contract number: 2016/01343-7 to R.A.K.), Fundacao de Amparo a Pesquisa do Estado do Rio de Janeiro - Brazil (grant number: E-26/201.277/2021 to L.S.B.) and Inova Fiocruz/ Fundacao Oswaldo Cruz - Brazil (grant number: 48401485034116) to L.S.B., O.G.C. and M.G.d.F.C. The funding agencies had no role in the conceptualization of the study.

LANCET REGIONAL HEALTH-AMERICAS 17, 100397, 2023. DOI: 10.1016/j.lana.2022.100397

[P114-2023] "Europium induced point defects in SrSnO3--based perovskites employed as antibacterial agents"

Chantelle, L.; Kennedy, B. J.; Oliveira, C. P. de; Gouttefangeas, F.; Siu-Li, M.; **Landers, R.***; Ciorita, A.; Rostas, A. M.; Santos, I. M. G. dos; Oliveira, A. L. M. de

The antibacterial activity of Eu3+-doped SrSnO3-type materials against Staphylococcus aureus (Gram-posi-tive) and Escherichia coli (Gram-negative) bacteria is described. Two Eu3+--doped SrSnO3 perovskites -(SrEu) SnO3 and Sr(SnEu)O3 -were synthesised by a modified-Pechini method and characterised by XRD, FT-IR, FE-SEM, HR-STEM/EDX, BET, Photoluminescence (PL), UV-Vis, Q-band EPR and XPS to understand the impact of Eu doping on the materials' properties. Structural characterisations indicated that the desired perovskite phase completely crystallised after calcination at 700 degrees C. Long and short-range structural changes were observed as a function of the site-doping with Eu and calcination temperature. Small specific surface area, which varied from 8.09 to 13.28 m2/g, was observed for the samples. Nonetheless, the formation of na-noparticles under 10 nm, clusters of nanoparticles > 100 nm, and nanorods with 100-600 nm x 10-50 nm (length x width) was evidenced. Eu3+ doping led to an increase of Sn2+ and oxygen vacancies in SrSnO3 lattice, playing an essential role in the antibacterial activity. Reduced Eu2+ species were also observed. The samples had activity below 5 % against Escherichia coli, whereas (SrEu)SnO3 displayed an efficiency of 100 % after 24 h against Staphylococcus aureus at a concentration of 1 mg/mL. Our results demonstrate that a specific chemical doping with Eu induces the formation of distinct point defect (Sn2+, Eu2+ and VO center dot) in the materials, which promoted a negative surface charge that seems to have improved the redox ability and, therefore, enhanced the biocide property.

JOURNAL OF ALLOYS AND COMPOUNDS 956, 170353, 2023. DOI: 10.1016/j.jallcom.2023.170353

[P115-2023] "First-principles and reactive molecular dynamics study of the elastic properties of pentahexoctite-based nanotubes"

Brandao, W. H. S.; **Sousa, J. M. de***; Aguiar, A. L.; **Galvao, D. S.***; Ribeiro, L. A.; **Fonseca, A. F.***

Pentahexoctite (PH) is a pure sp2 hybridized planar carbon allotrope whose structure consists of a symmetric combination of pentagons, hexagons, and octagons. The proposed PH structure was shown to be an intrinsically metallic material exhibiting good mechanical and thermal stability. PH nanotubes (PHNTs) have also been proposed, and their properties were obtained from first principles calculations. Here, we carried out fully-atomistic simulations, combining reactive (ReaxFF) molecular dynamics (MD) and density functional theory (DFT) methods, to study the PHNTs elastic properties and fracture patterns. We have investigated the mechanical properties behavior as a function of the tube diameter and temperature regimes. Our results showed that the PHNTs, when subjected to large tensile strains, undergo abrupt structural transitions exhibiting brittle fracture patterns without a plastic regime.

MECHANICS OF MATERIALS 183, 104694, 2023. DOI: 10.1016/j.mechmat.2023.104694

[P116-2023] "Full Heusler Fe2CrAl nanogranular films produced by pulsed laser deposition for magnonic applications"

Andrade, V. M.; Checca, N. R.; Paula, V. G. de; **Pirota, K. R.*;** Rossi, A. L.; Garcia, F.; Vovk, A.; Bunyaev, S. A.; Kakazei, G. N.

Obtaining Heusler alloys at the nanoscale with good crystallographic features is appealing for a large range of technological applications, from biomedical to spintronics devices. In particular, Fe2CrAl as bulk is known to present magnetic properties that are strongly sensitive to chemical and physical constraints, such as structural disorder and chemical composition. We report a throughout structural, morphological, and magnetic characterization of Fe2CrAl Heusler nanoparticles obtained by pulsed laser deposition technique. The nanoparticles are composed of slightly off-stoichiometric grains with two distinct morphologies where the role of chemical disorder and inhomogeneity on the magnetic behavior was evaluated. Through DC magnetization measurements, a superparamagnetic behavior is observed and a Gilbert damping of 9 x 10(-3) is acquired from broadband ferromagnetic resonance data, which is comparable with standard materials used for magnonics applications. We discuss the complex magnetostructural coupling that rises on the nanoparticle system, comparing these results with the stoichiometric Fe2CrAl bulk target behavior.

JOURNAL OF APPLIED PHYSICS 134[2], 023901, 2023. DOI: 10.1063/5.0151291

[P117-2023] "Hidden physics in the decays of pions and other mesons"

Guzzo, M. M.*; Leite, L. J. F.*; Novelo, S. W. P.*; Peres, O. L. G.*; Pleitez, V.

It has been commonly assumed that pseudoscalar contributions to the leptonic decay of charged mesons, like pions and kaons, is strongly constrained due to the helicity suppression present in the ratio Rl/l' = Gamma(P -lv[y])/Gamma(P -l'v[y]), where P are the charged pseudoscalar meson and l; l' = e, mu, T. Here we show that if the effective couplings are proportional to the corresponding charged lepton masses (and also the Pontecorvo-Maki-Nakagawa-Sakata (PMNS) matrix), the constraints from Rl/l' are entirely avoided, and a rather new large allowed region is permitted in the parameter space. In the case of the electron, we found a nontrivial region in the range 10-4 less than or similar to (GI/GF) less than or similar to 10-3, where GI is the effective pseudoscalar coupling associated with a novel charged scalar field, I, and GF is the Fermi constant. Furthermore, we show that this dependence of the pseudoscalar couplings on the charged lepton masses can naturally be associated with a critical class beyond the standard model physics, namely models without (leptonic) flavor-changing neutral currents in the scalar sector. The most known examples are the models that satisfy the so-called Glashow-Weinberg-Paschos theorem. Finally, we also point out that, in those cases, the decay rate is degenerated with the Standard Model prediction, possibly hiding the new physics effects in those decays.

PHYSICAL REVIEW D 107[9], 095037, 2023. DOI: 10.1103/PhysRevD.107.095037

[P118-2023] "Highly-parallelized simulation of a pixelated LArTPC on a GPU"

Abud, A. A.; Abi, B.; **Adriano, C.*; Bazetto, M. C. Q.*; Belchior, E.*; Aguiar, R. de*; Almeida, P. de*; Holanda, P. C. de*; Souza, G. de*; Gelli, B.*; Giammaria, P.*; Guzzo, M. M.*; Kemp, E.*; Machado, A. A.*; Peres, O. L. G.*; Pimentel, V. L.*; Prakash, S.*; Segreto, E.***; et al. DUNE Collaboration

The rapid development of general-purpose computing on graphics processing units (GPGPU) is allowing the implementation of highly-parallelized Monte Carlo simulation chains for particle physics experiments. This technique is particularly suitable for the simulation of a pixelated charge readout for time projection chambers, given the large number of channels that this technology employs. Here we present the first implementation of a full microphysical simulator of a liquid argon time projection chamber (LArTPC) equipped with light readout and pixelated charge readout, developed for the DUNE Near Detector. The software is implemented with an end-to-end set of GPU--optimized algorithms. The algorithms have been written in Python and translated into CUDA kernels using Numba, a just-in-time compiler for a subset of Python and NumPy instructions. The GPU implementation achieves a speed up of four orders of magnitude compared with the equivalent CPU version. The simulation of the current induced on 103 pixels takes around 1 ms on the GPU, compared with approximately 10 s on the CPU. The results of the simulation are compared against data from a pixel-readout LArTPC prototype.

JOURNAL OF INSTRUMENTATION 18[4], P04034, 2023. DOI: 10.1088/1748-0221/18/04/P04034

[P119-2023] "Identification and reconstruction of low-energy electrons in the ProtoDUNE-SP detector"

Abud, A. A.; Abi, B.; **Adriano, C.*; Bazetto, M. C. Q.*; Belchior, E.*; Aguiar, R. de*; Almeida, P. de*; Holanda, P. C. de*; Souza, G. de*; Gelli, B.*; Giammaria, P.*; Guzzo, M. M.*; Kemp, E.*; Machado, A. A.*; Peres, O. L. G.*; Pimentel, V. L.*; Prakash, S.*; Segreto, E.***; et al. DUNE Collaboration

Measurements of electrons from ?e interactions are crucial for the Deep Underground Neutrino Experiment (DUNE) neutrino oscillation program, as well as searches for physics beyond the standard model, supernova neutrino detection, and solar neutrino measurements. This article describes the selection and reconstruction of low-energy (Michel) electrons in the ProtoDUNE-SP detector. ProtoDUNE-SP is one of the prototypes for the DUNE far detector, built and operated at CERN as a charged particle test beam experiment. A sample of low-energy electrons produced by the decay of cosmic muons is selected with a purity of 95%. This sample is used to calibrate the low-energy electron energy scale with two techniques. An electron energy calibration based on a cosmic ray muon sample uses calibration constants derived from measured and simulated cosmic ray muon events. Another calibration technique makes use of the theoretically well-understood Michel electron energy spectrum to convert reconstructed charge to electron energy. In addition, the effects of detector response to low-energy electron energy scale and its resolution including readout electronics threshold effects are quantified. Finally, the relation between the theoretical and reconstructed low-energy electron energy spectra is derived, and the energy resolution is characterized. The low-energy electron selection presented here accounts for about 75% of the total electron deposited energy. After the addition of lost energy using a Monte Carlo simulation, the energy resolution improves from about 40% to 25% at 50 MeV. These results are used to validate the expected capabilities of the DUNE far detector to reconstruct low-energy electrons.

PHYSICAL REVIEW D 107[9], 2023. DOI: 10.1103/PhysRevD.107.092012

[P120-2023] "Impacts of dielectric screening on the luminescence of monolayer WSe2"

Costa, F. J. R.*; Brito, T. G. L.*; Barcelos, I. D.; **Zagonel, L. F.***

Single layers of transition metal dichalcogenides (TMDCs), such as WSe2 have gathered increasing attention due to their intense electron-hole interactions, being considered promising candidates for developing novel optical applications.

Within the few-layer regime, these systems become highly sensitive to the surrounding environment, enabling the possibility of using a proper substrate to tune desired aspects of these atomically-thin semiconductors. In this scenario, the dielectric environment provided by the substrates exerts significant influence on electronic and optical properties of these layered materials, affecting the electronic band-gap and the exciton binding energy. However, the corresponding effect on the luminescence of TMDCs is still under discussion. To elucidate these impacts, we used a broad set of materials as substrates for single-layers of WSe2, enabling the observation of these effects over a wide range of electrical permittivities. Our results demonstrate that an increasing permittivity induces a systematic red-shift of the optical band-gap of WSe2, intrinsically related to a considerable reduction of the luminescence intensity. Moreover, we annealed the samples to ensure a tight coupling between WSe2 and its substrates, reducing the effect of undesired adsorbates trapped in the interface. Ultimately, our findings reveal how critical the annealing temperature can be, indicating that above a certain threshold, the heating treatment can induce adverse impacts on the luminescence. Furthermore, our conclusions highlight the influence the dielectric properties of the substrate have on the luminescence of WSe2, showing that a low electrical permittivity favours preserving the native properties of the adjacent monolayer.

NANOTECHNOLOGY 34[38], 385703, 2023. DOI: 10.1088/1361-6528/acda3b

[P121-2023] "In Silico Evaluation of the Binding Energies of Androgen Receptor Agonists in Wild-Type and Mutational Models"

Albuquerque, A. C. C.; Bezerra, K. S.; Vianna, J. D.; Batista, S. O.; Lima Neto, J. X. de; Campos, D. M. de O.; Oliveira, J. I. N.; **Galvao, D. S.*; Fulco, U. L.***

Resumo characteristics. Among the many side effects of hormonetherapy with AAS, the following stand out: heart problems, adrenalgland disorders, aggressive behavior, increased risk of prostate cancer,problems related to lack of libido and impotence. Such substancesvary in the relationship between androgenic activity, and the activationof the androgen receptor (AR) is of fundamental importance for thesingularity of the action of each AAS. In this sense, our study evaluatesthe aspects that comprise the interactions of testosterone agonists(TES), dihydrotestosterone (DHT) and tetrahydrogestrinone (THG) incomplex with the AR. In addition, we also evaluated the impact ofligand-receptor affinity differences in a mutation model. Weapply computational techniques based on density functional theory(DFT) and use, as methodology, Molecular Fractionation with ConjugateCaps (MFCC). The energetic specificities present in the interactionbetween the analyzed complexes attest that the highest affinity withthe AR receptor is found for AR--THG, followed by AR-DHT,AR-TES and AR-T877A-DHT, respectively. Our results alsoshow the differences and equivalences between the different agonists,in addition to evaluating the difference between the DHT ligand incomplex with the wild--type and mutant receptor, presenting the mainamino acid residues that involve the interaction with the ligands.The computational methodology used proves to be an operative and sophisticatedchoice to help in the search for pharmacological agents for varioustherapies that have androgen as a target.

JOURNAL OF PHYSICAL CHEMISTRY B 127[22], 5005-5017, 2023. DOI: 10.1021/acs.jpcb.3c01103

[P122-2023] "Information visualization and machine learning driven methods for impedimetric biosensing"

Shimizu, F. M.*; Barros, A. de*; Braunger, M. L.*; Gaal, G.*; Riul, A.*

This review addresses the convergence of impedimetric biosensing technologies and computational methods facilitating data information visualization. The literature brings various methodologies and analytical techniques associated with impedance measurements for biosensing, ranging from versatile testing platforms to management decisions according to the reported detection level. To this end, there has been a growing need for multivariate methods in data analysis, with a steady increase in machine learning methods to determine biosensing parameters. It has been expanded to calibration, analysis, classification, regression procedures, and more recently, calibration space and data inspection rules to optimize the device performance. Consequently, there has been a significant improvement in the automation and accuracy of data, with immediate impacts on diagnostics and protocols in recent years. We focus here on impedimetric biosensing and how multivariate methods combined with machine learning tools (artificial neural network, random forest, decision three, support vector machine, etc.) contribute to the outstanding performance of these devices.

TRAC-TRENDS IN ANALYTICAL CHEMISTRY 165, 117115, 2023. DOI: 10.1016/j.trac.2023.117115

[P123-2023] "Investigation of K plus K- interactions via femtoscopy in Pb-Pb collisions at root sNN=2.76 TeV at the CERN Large Hadron Collider"

Acharya, S.; Adamova, D.; **Chinellato, D. D.*; Guardiano, G. G.*; Jahnke, C.*; Takahashi, J.***; et al. ALICE Collaboration

Femtoscopic correlations of nonidentical charged kaons (K+K-) are studied in Pb-Pb collisions at a center-of -mass energy per nucleon-nucleon collision root sNN = 2.76 TeV by ALICE at the CERN Large Hadron Collider. One-dimensional K+K- correlation functions are analyzed in three centrality classes and eight intervals of particle-pair transverse momentum. The LednickATIN SMALL LETTER Y WITH ACUTE and Luboshitz interaction model used in the K+K- analysis includes the final-state Coulomb interactions between kaons and the final-state interaction through a0(980) and f0(980) resonances. The mass of f0(980) and coupling were extracted from the fit to K+K- correlation functions using the femtoscopic technique. The measured mass and width of the f0(980) resonance are consistent with other published measurements. The height of the phi(1020) meson peak present in the K+K- correlation function rapidly decreases with increasing source radius, qualitatively in agreement with an inverse volume dependence. A phenomenological fit to this trend suggests that the phi(1020) meson yield is dominated by particles produced directly from the hadronization of the system. The small fraction subsequently produced by final--state interactions could not be precisely quantified with data presented in this paper and will be assessed in future work.

PHYSICAL REVIEW C 107[5], 054904, 2023. DOI: 10.1103/PhysRevC.107.054904

[P124-2023] "Ion pair and larger ion cluster formation in water interfacial regions: An atomic force microscopy study"

Teschke, O.*; Soares, D. M.*

Interfacial regions attached to hydrophobic and hydrophilic surfaces have very low relative permittivities (epsilon similar to 3-5), and these low values induce the formation of ion pairs. A detailed description of ion pairing will be possible only after the development of adequate experimental probing methods. The scheme described in this work detects the ion pair (or multistage ion association) formation in water solutions in the interfacial region. Forces acting on the tip when immersed in the interfacial region attached to hydrophilic substrates, such as mica where epsilon < 7, are attractive (AFM tip dielectric constant = 7).

These attractive force steps with extensions equal or smaller than the Bjerrum length at hydrophilic substrates are associated with ion pair formation in interfacial regions. Measurements show that the interfacial water molecular arrangement and ion pairs form an ordered structure (epsilon < 7) induced by mica interfacial charges. The interfacial region attached to hydrophobic substrates, however, form separated arrangements of ion pairs and water molecular structures as observed by the repulsive steps (epsilon > 7) intercalated in between attractive regions (epsilon < 7). (c) 2023 Author(s). All article content, except where otherwise noted, is licensed under a Creative Commons Attribution (CC BY) license (http://creativecommons.org/licenses/by/4.0/).

AIP ADVANCES 13[7], 075319, 2023. DOI: 10.1063/5.0141351

[P125-2023] "Joint analysis of Dark Energy Survey Year 3 data and CMB lensing and cosmological constraints"

Chang, C.; Omori, Y.; **Navarro-Alsina, A.***; et al.

Cross-correlations of galaxy positions and galaxy shears with maps of gravitational lensing of the cosmic microwave background (CMB) are sensitive to the distribution of large-scale structure in the Universe. Such cross-correlations are also expected to be immune to some of the systematic effects that complicate correlation measurements internal to galaxy surveys. We present measurements and modeling of the cross--correlations between galaxy positions and galaxy lensing measured in the first three years of data from the Dark Energy Survey with CMB lensing maps derived from a combination of data from the 2500 deg2 SPT-SZ survey conducted with the South Pole Telescope and full-sky data from the Planck satellite. The CMB lensing maps used in this analysis have been constructed in a way that minimizes biases from the thermal Sunyaev Zel'dovich effect, making them well suited for cross--correlation studies. The total signal-to-noise of the cross-correlation measurements is 23.9 (25.7) when using a choice of angular scales optimized for a linear (nonlinear) galaxy bias model. We use the cross-correlation measurements to obtain constraints on cosmological parameters. For our fiducial galaxy sample, which consist of four bins of magnitude-selected galaxies, we find constraints of omega m 1/4 0.272 thorn 0.032 pffiffffffffffffffffffffffffffffffffi-0.052 and S8 equivalent to sigma 8 omega m=0.3 1/4 0.736 thorn 0.032 -0.028 (omega m 1/40.245 thorn 0.0-0.04426 and S8 1/40.734 thorn 0.035 -0.028) when assuming linear (nonlinear) galaxy bias in our modeling. Considering only the cross-correlation of galaxy shear with CMB lensing, we find omega m 1/4 0.270 thorn 0.043 -0.061 and S8 1/4 0.740 thorn 0.034 -0.029 . Our constraints on S8 are consistent with recent cosmic shear measurements, but lower than the values preferred by primary CMB measurements from Planck.

PHYSICAL REVIEW D 107[2], 023530, 2023. DOI: 10.1103/PhysRevD.107.023530

[P126-2023] "Joint analysis of Dark Energy Survey Year 3 data and CMB lensing from SPT and Planck. I. Construction of CMB lensing maps and modeling choices"

Omori, Y.; Baxter, E. J.; Cheng, C.; Friedrich, O.; **Navarro--Alsina, A.*; et al.**

Joint analyses of cross-correlations between measurements of galaxy positions, galaxy lensing, and lensing of the cosmic microwave background (CMB) offer powerful constraints on the large-scale structure of the Universe. In a forthcoming analysis, we will present cosmological constraints from the analysis of such cross-correlations measured using Year 3 data from the Dark Energy Survey (DES), and CMB data from the South Pole Telescope (SPT) and Planck. Here we present two key ingredients of this analysis: (1) an improved CMB lensing map in the SPT-SZ survey footprint and (2) the analysis methodology that will be used to extract cosmological information from the cross-correlation measurements. Relative to previous lensing maps made from the same CMB observations, we have implemented techniques to remove contamination from the thermal Sunyaev Zel'dovich effect, enabling the extraction of cosmological information from smaller angular scales of the cross-correlation measurements than in previous analyses with DES Year 1 data. We describe our model for the cross-correlations between these maps and DES data, and validate our modeling choices to demonstrate the robustness of our analysis. We then forecast the expected cosmological constraints from the galaxy survey--CMB lensing auto and cross-correlations. We find that the galaxy-CMB lensing and galaxy shear-CMB lensing correlations will on their own provide a pffiffffffffffffffffffffffffffffffffficonstraint on S8 1/4 sigma 8 omega m=0.3 at the few percent level, providing a powerful consistency check for the DES-only constraints. We explore scenarios where external priors on shear calibration are removed, finding that the joint analysis of CMB lensing cross-correlations can provide constraints on the shear calibration amplitude at the 5% to 10% level.

PHYSICAL REVIEW D 107[2], 023529, 2023. DOI: 10.1103/PhysRevD.107.023529

[P127-2023] "Joint analysis of Dark Energy Survey Year 3 data and CMB lensing from SPT and Planck. III. Combined cosmological constraints"

Abbott, T. M. C.; Aguena, M.; **Navarro-Alsina, A.***; et al.

We present cosmological constraints from the analysis of two--point correlation functions between galaxy positions and galaxy lensing measured in Dark Energy Survey (DES) Year 3 data and measurements of cosmic microwave background (CMB) lensing from the South Pole Telescope (SPT) and Planck. When jointly analyzing the DES-only two-point functions and the DES cross--correlations with SPT + Planck CMB lensing, we find Omega(m) = 0.344 + 0.030 and S-8 equivalent to sigma(8)(Omega(m)/0.3) (0.5) = 0.773 +/- 0.016, assuming Lambda CDM. When additionally combining with measurements of the CMB lensing autospectrum, we find omega m = 0.306(-0.021)(+0.018) and S-8 = 0.792 +/- 0.012. The high signal-to-noise of the CMB lensing cross-correlations enables several powerful consistency tests of these results, including comparisons with constraints derived from cross-correlations only, and comparisons designed to test the robustness of the galaxy lensing and clustering measurements from DES. Applying these tests to our measurements, we find no evidence of significant biases in the baseline cosmological constraints from the DES-only analyses or from the joint analyses with CMB lensing cross-correlations. However, the CMB lensing cross-correlations suggest possible problems with the correlation function measurements using alternative lens galaxy samples, in particular the REDMAGIC galaxies and high-redshift MAGLIM galaxies, consistent with the findings of previous studies. We use the CMB lensing cross-correlations to identify directions for further investigating these problems.

PHYSICAL REVIEW D 107[2], 023531, 2023. DOI: 10.1103/PhysRevD.107.023531

[P128-2023] "Limits to Gauge Coupling in the Dark Sector Set by the Nonobservation of Instanton-Induced Decay of Super-Heavy Dark Matter in the Pierre Auger Observatory Data"

Arbeletche, L. B.*; **Chinellato, J. A.*; Franco, D. de O.*; Dobrigkeit, C.*; Fauth, A. C.*; Payeras, A. M.*; Muller, M. A.***; et al. Pierre Auger Collaboration

Instantons, which are nonperturbative solutions to Yang-Mills equations, provide a signal for the occurrence of quantum tunneling between distinct classes of vacua. They can give rise to decays of particles otherwise forbidden. Using data collected at the Pierre Auger Observatory, we search for signatures of such instanton-induced processes that would be suggestive of super--heavy particles decaying in the Galactic halo. These particles could have been produced during the post-inflationary epoch and match the relic abundance of dark matter inferred today. The nonobservation of the signatures searched for allows us to derive a bound on the reduced coupling constant of gauge interactions in the dark sector: alpha X < 0.09, for 109 < MX=GeV < 1019. Conversely, we obtain that, for instance, a reduced coupling constant alpha X = 0.09 excludes masses MX greater than or similar to 3 x 1013 GeV. In the context of dark matter production from gravitational interactions alone, we illustrate how these bounds are complementary to those obtained on the Hubble rate at the end of inflation from the nonobservation of tensor modes in the cosmological microwave background.

PHYSICAL REVIEW LETTERS 130[6], 061001, 2023. DOI: 10.1103/PhysRevLett.130.061001

[P129-2023] "Magnetic behavior of two-dimensional manganese telluride"

Gowda, C. C.; **Tromer, R.***; Pandey, P.; Chandravanshi, D.; Chandra, A.; Chattopadhyay, K.; **Galvao, D. S.***; Tiwary, C. S.

Magnetism in atomically thin two-dimensional (2D) materials is attractive for several applications such as memory devices, sensors, biomedical devices, etc. Here, we have synthesized 2D manganese telluride (MnTe) using a scalable synthesis method consisting of melting followed by liquid phase exfoliation. Both bulk and 2D MnTe samples were analyzed for their magnetic behavior at room temperature (RT) and lower temperatures (10 K). A change from antiferromagnetic (AFM) to paramagnetic (PM) behavior was observed in 2D MnTe flakes. Enhanced magnetic saturation values (up to 400% increase) were observed as compared to bulk MnTe in RT. Density functional theory simulations explain the layer--dependent magnetic behavior of the 2D MnTe flakes, as well the AFM to PM transition due to an unbalanced spin population.

2D MATERIALS 10[4], 045006, 2023. DOI: 10.1088/2053-1583/

[P130-2023] "Magnetic Field Fiber Specklegram Sensors Based on Tb3+-Doped Magneto-Optical Glasses With High Verdet Constants"

Cabral, T. D.; Franco, D. F.; Fujiwara, E.; Nalin, M.; **Cordeiro, C. M. B.***

Optical fiber specklegram sensors (FSSs) for magnetic field measurements are reported. The probes are compact, with only a fiber length of similar to 100 mm exposed to a magnetic field and comprised of no-core fibers doped with terbium oxide (Tb4O7), so the Verdet constant is dramatically improved in comparison to regular commercial fibers (similar to 20x increase, 10-mol% fiber), greatly enhancing the modulation of the output specklegram. The response to static magnetic fields was evaluated for different concentrations (6-10 mol%) of Tb4O7, yielding an increase in sensitivity of up to 59x (8.78 x 10(-2) mT(-1), 10 mol%) and 6x resolution (1.86 x 10(-2) mT, 6 mol%) in relation to a regular silica multimode fiber (MMF). A simple setup with a He-Ne laser and inexpensive webcam charge-coupled device (CCD) camera was employed, producing results comparable to fiber sensors based on more complicated setups such as fiber interferometers. To the best of our knowledge, this comprises the first demonstration of highly multimode magnetic field FSS based on magneto-optical (MO) glass to capitalize on both the Faraday rotation and the polarization mode conversion.

IEEE SENSORS JOURNAL 23[7], 6872-6879, 2023. DOI: 10.1109/JSEN.2023.3244120

[P131-2023] "Measurement of anti-He-3 nuclei absorption in matter and impact on their propagation in the Galaxy"

Acharya, S.; Adamova, D.; **Chinellato, D. D.*; Guardiano, G. G*.; Jahnke, C.*; Takahashi, J.***; et al. ALICE Collaboration

In our Galaxy, light antinuclei composed of antiprotons and antineutrons can be produced through high-energy cosmic-ray collisions with the interstellar medium or could also originate from the annihilation of dark-matter particles that have not yet been discovered. On Earth, the only way to produce and study antinuclei with high precision is to create them at high-energy particle accelerators. Although the properties of elementary antiparticles have been studied in detail, the knowledge of the interaction of light antinuclei with matter is limited. We determine the disappearance probability of (3)(He) over bar when it encounters matter particles and annihilates or disintegrates within the ALICE detector at the Large Hadron Collider. We extract the inelastic interaction cross section, which is then used as an input to the calculations of the transparency of our Galaxy to the propagation of (3)(He) over bar stemming from dark-matter annihilation and cosmic-ray interactions within the interstellar medium. For a specific dark-matter profile, we estimate a transparency of about 50%, whereas it varies with increasing (3)(He) over bar momentum from 25% to 90% for cosmic-ray sources. The results indicate that (3)(He) over bar nuclei can travel long distances in the Galaxy, and can be used to study cosmic-ray interactions and dark-matter annihilation.

NATURE PHYSICS 19[1], 61-+, 2023. DOI: 10.1038/s41567-022-01804-8

[P132-2023] "Measuring exciton-phonon coupling in semiconductor nanocrystals"

Liu, A.; **Almeida, D. B.***; Cundiff, S. T.; **Padilha, L. A.***

At low excitation density, the dynamics of excitons in semiconductor nanocrystals are largely dictated by their interactions with the underlying atomic lattice. This exciton-phonon coupling (EPC) is responsible, for example, for absorption and luminescence linewidths at elevated temperatures, relaxation processes following optical excitation, and even degradation of quantum coherent applications. Characterizing and understanding EPC is therefore central to guiding rational design of colloidal nanocrystal materials and their device applications. In this review, we compare different spectroscopic methods of measuring exciton-phonon interactions and the complementary information that they provide. We emphasize the development of a new technique, termed multidimensional coherent spectroscopy, that circumvents many of the limitations of traditional methods.

ELECTRONIC STRUCTURE 5[3], 033001, 2023. DOI: 10.1088/2516-1075/acde2a

[P133-2023] "Mechanical, Electronic, and Optical Properties of 8-16-4 Graphyne: A 2D Carbon Allotrope with Dirac Cones"

Tromer, R. M.*; Pereira Jr., M. L. L.; Lima, K. A. L.; **Fonseca, A. F.***; Silva, L. R. da; **Galvao, D. S.***; Ribeiro Jr., L. A.

Graphene's success has led to the theoreticalpredictionand experimental synthesis of various 2D carbon-based allotropes.To explore the mechanical, structural, electronic, and optical propertiesof 8-16-4 graphyne, we employed density functional theory using theGGA/PBE approach, ab initio molecular dynamics (AIMD), and classicalreactive molecular dynamics simulations.

Our AIMD results indicatethat this material demonstrates excellent dynamical and thermal stabilities.It has a formation energy of -8.57 eV/atom and an elastic moduliof 262.37 GPa. Regarding its band structure, this graphyne analogueis a semimetal with two Dirac cones. It also exhibits transparencyand intense optical activity in the infrared region. Notably, theband structure of 8-16-4 graphyne remains practically unchanged atmoderate strain regimes. To our knowledge, this is the first known2D carbon allotrope to exhibit such behavior.

JOURNAL OF PHYSICAL CHEMISTRY C 127[25], 12226-12234, 2023. DOI: 10.1021/acs.jpcc.3c01788

[P134-2023] "Multiferroic Electroactive Polymer Blend/Ferrite Nanocomposite Flexible Films for Cooling Devices"

Thandapani, P.; Aepuru, R.; **Beron, F.***; Viswanathan, M. R.; Varaprasad, K.; Zabotto, F. L.; Jimenez, J. A.; Denardin, J. C.

In recent days, the interest toward the development ofmulticaloricmaterials for cooling application is increasing, whereas multiferroicmaterials would be the suitable alternative to the conventional refrigerants.To explore them, the poly(methyl methacrylate)/poly(vinylidenefluoride-co-hexafluoropropylene) (PMMA/PVDF-HFP) blend and PMMA/PVDF-HFP/Zn0.5Cu0.5Fe2O4 flexible multiferroicnanocomposite films were fabricated by the solution casting method.The structural analyses prove that the strong interfacial interactionbetween the PMMA/PVDF-HFP blend and the Zn0.5Cu0.5Fe2O4 (ZCF) through hydroxyl (-OH) andcarbonyl group bonding with PVDF-HFP enhanced the thermal stabilityand suppressed the electroactive & beta; phase from 67 to 62%. Experimentalresults show that 10 wt % of superparamagnetic ZCF nanoparticles witha particle size of 6.8 nm induced both the magnetocaloric and magnetoelectriceffects in a nonmagnetic PMMA/PVDF-HFP ferroelectric matrix at roomtemperature. A set of isothermal magnetization curves were recordedin the magnetic field strength of 0-40 kOe and a temperaturerange of 2-400 K. The maximum magnetic entropy changes (& UDelta;S (M)) of -0.69 J & BULL;kg(-1) K-1 of ZCF nanoparticles and -0.094 J & BULL;kg(-1) K-1 of PMMA/PVDF-HFP/ZCF nanocompositesshowed an interesting table-like flat variation in the temperaturerange of 100-400 K as a function of the magnetic field. Thesamples display a large temperature span with a relative cooling power of 293 and 40 J & BULL;kg(-1) for ZCF and PMMA/PVDF-HFP/ZCF,respectively. The magnetoelectric effect of the PMMA/PVDF-HFP/ZCFcomposite was proved, but it generated only 1.42 mV/m & BULL;Oe in theapplied field of 5 kOe. Hence, the entropy change of the present nanocompositewas only due to the magnetocaloric effect, where the magnetoelectriccross-coupling coefficient was negligible. The multicaloric effectcould be established if the nanocomposite showed a larger magnetoelectriccross-coupling in addition to the magnetocaloric effect. This approachprovides the research findings in functional multiferroic polymernanocomposites for miniaturized cooling devices.

ACS APPLIED POLYMER MATERIALS 5[8], 5926-5936, 2023. DOI: 10.1021/acsapm.3c00589

[P135-2023] "Non-local contribution from small scales in galaxy-galaxy lensing: comparison of mitigation schemes"

Prat, J.; Zacharegkas, G.; Park, Y.; **Navarro-Alsina, A.***; et al. DES Collaboration

Recent cosmological analyses with large-scale structure and weak lensing measurements, usually referred to as 3 x 2pt, had to discard a lot of signal to noise from small scales due to our inability to accurately model non-linearities and baryonic effects. Galaxy-galaxy lensing, or the position-shear correlation between lens and source galaxies, is one of the three two-point correlation functions that are included in such analyses, usually estimated with the mean tangential shear. However, tangential shear measurements at a given angular scale theta or physical scale R carry information from all scales below that, forcing the scale cuts applied in real data to be significantly larger than the scale at which theoretical uncertainties become problematic. Recently, there have been a few independent efforts that aim to mitigate the non-locality of the galaxy-galaxy lensing signal. Here, we perform a comparison of the different methods, including the Y-transformation, the point-mass marginalization methodology, and the annular differential surface density statistic. We do the comparison at the cosmological constraints level in a combined galaxy clustering and galaxy-galaxy lensing analysis. We find that all the estimators yield equivalent cosmological results assuming a simulated Rubin Observatory Legacy Survey of Space and Time (LSST) Year 1 like set-up and also when applied to DES Y3 data. With the LSST Y1 set-up, we find that the mitigation schemes yield similar to 1.3 times more constraining S-8 results than applying larger scale cuts without using any mitigation scheme.

MONTHLY NOTICES OF THE ROYAL ASTRONOMICAL SOCIETY 522[1], 412-425, 2023. DOI: 10.1093/mnras/stad847

[P136-2023] "Observation of electroweak W+W- pair production in association with two jets in proton-proton collisions at root s=13 TeV"

Tumasyan, A.; Adam, W.; **Chinellato, J. A.***; et al.

An observation is reported of the electroweak production of a W+W- pair in association with two jets, with both W bosons decaying leptonically. The data sample corresponds to an integrated luminosity of 138 fb(-1) of proton-proton collisions at root s =13 TeV, collected by the CMS detector at the CERN LHC. Events are selected by requiring exactly two opposite-sign leptons (electrons or muons) and two jets with large pseudorapidity separation and high dijet invariant mass. Events are categorized based on the flavor of the final-state leptons. A signal is observed with a significance of 5.6 standard deviations (5.2 expected) with respect to the background-only hypothesis. The measured fiducial cross section is 10.2 +/- 2.0 fb and this value is consistent with the standard model prediction of 9.1 +/- 0.6 fb.

PHYSICS LETTERS B 841, 137495, 2023. DOI: 10.1016/j.physletb.2022.137495

[P137-2023] "Observation of the two-photon transition enhanced first hyperpolarizability spectra in cinnamaldehyde derivatives: A femtosecond regime study"

Santos, C. H. D. dos; Cocca, L. Z. H.; Pelosi, A. G.; Batista, V. F.; Pinto, D. C. G. A.; Faustino, M. A. F.; Vivas, M. G.; **Siqueira, J. D. de P.***; Mendonca, C. R.; De Boni, L.

The application of nonlinear optical effects in optoelectronic devices is still scarce because the irradiance threshold necessary to induce a specific effect is very high. In this context, knowing the frequency-resolved first order molecular hyperpolarizability (beta) is essential to identifying regions where this response is intense enough to allow for applications in commercial devices. Thus, herein, we have determined the beta spectral dependence of five new push-pull cinnamylidene acetophenone derivatives using femtosecond laser-induced Hyper-Rayleigh Scattering (HRS). A considerable increase in beta values was observed in molecules. We found remarkable beta values in regions near the two-photon resonance, which are mediated by electron withdrawing and donating groups. This effect was mapped using wavelength-tunable femtosecond Z-scan technique.

Furthermore, it was modeled in light of the sum-over--states approach for the second- and third-order nonlinearities. Finally, our outcomes suggest a strategy to obtain large beta values mediated by the 2PA transition.

JOURNAL OF CHEMICAL PHYSICS 158[21], 214201, 2023. DOI: 10.1063/5.0151622

[P138-2023] "Optics in South America: introduction"

Wiederhecker, G. S.*; Cavalcanti, S. B.; Fontes, A.; Gacia-Suerquia, J.; Perez, D.; Vera, E.; Bragas, A.; Matos, C. de; Fainstein, A.; Felinto, D.; Milori, D. M. B. P.; Walborn, S. P.

South American optics research has seen remarkable growth over the past 50 years, with significant contributions in areas such as quantum optics, holography, spectroscopy, nonlinear optics, statistical optics, nanophotonics and integrated photonics. The research has driven economic development in sectors like telecom, biophotonics, biometrics, and agri-sensing. This joint feature issue between JOSA A and JOSA B exhibits cutting-edge optics research fromthe region, fostering a sense of community and promoting collaboration among researchers.

JOURNAL OF THE OPTICAL SOCIETY OF AMERICA B-OPTICAL PHYSICS 40[4], 2023. OSA1-OSA2, 2023. DOI: 10.1364/JOSAB.491703

[P139-2023] "Parametrically driving a quantum oscillator into exceptionality"

Downing, C. A.; **Vidiella-Barranco, A.***

The mathematical objects employed in physical theories do not always behave well. Einstein's theory of space and time allows for spacetime singularities and Van Hove singularities arise in condensed matter physics, while intensity, phase and polarization singularities pervade wave physics. Within dissipative systems governed by matrices, singularities occur at the exceptional points in parameter space whereby some eigenvalues and eigenvectors coalesce simultaneously. However, the nature of exceptional points arising in quantum systems described within an open quantum systems approach has been much less studied. Here we consider a quantum oscillator driven parametrically and subject to loss. This squeezed system exhibits an exceptional point in the dynamical equations describing its first and second moments, which acts as a borderland between two phases with distinctive physical consequences. In particular, we discuss how the populations, correlations, squeezed quadratures and optical spectra crucially depend on being above or below the exceptional point. We also remark upon the presence of a dissipative phase transition at a critical point, which is associated with the closing of the Liouvillian gap. Our results invite the experimental probing of quantum resonators under two-photon driving, and perhaps a reappraisal of exceptional and critical points within dissipative quantum systems more generally.

SCIENTIFIC REPORTS 13[1], 2023. DOI: 10.1038/s41598-023-37964-7

[P140-2023] "Precision measurement of the Z boson invisible width in pp collisions atN/s=13 TeV"

Tumasyan, A.; Adam, W.; **Chinellato, J. A.***; et al. CMS Collaboration

A precise measurement of the invisible width of the Z boson produced in proton-proton collisions at a center-of-mass energy of 13 TeV is presented using data recorded by the CMS experiment at the LHC, corresponding to an integrated luminosity of 36.3 fb-1. The result is obtained from a simultaneous fit to kinematic distributions for two data samples of Z boson plus jets: one dominated by Z boson decays to invisible particles and the other by Z boson decays to muon and electron pairs. The invisible width is measured to be 523 & PLUSMN; 3 (stat) & PLUSMN; 16 (syst) MeV. This result is the first precise measurement of the invisible width of the Z boson at a hadron collider, and is the single most precise direct measurement to date, competitive with the combined result of the direct measurements from the LEP experiments. & COPY; 2022 The Author(s). Published by Elsevier B.V. This is an open access article under the CC BY license (http://creativecommons .org /licenses /by /4 .0/). Funded by SCOAP3.

PHYSICS LETTERS B 842, 137563, 2023. DOI: 10.1016/j.physletb.2022.137563

[P141-2023] "Reproducibility analysis of functional connectivity measures for application in motor imagery BCIs"

Giarusso de Vazquez, P. F.*; Stefano Filho, C. A.*; Melo, G. C. de; Forner-Cordero, A.; **Castellano, G.***

Electroencephalography (EEG)-based motor imagery brain--computer interfaces (MI-BCIs) can improve motor rehabilitation processes. Nevertheless, the large variability of intra and inter-subject EEG signals has precluded translation of this technology to the clinical setting. The aim of this work was to evaluate the reproducibility of EEG functional connectivity (FC) features used to discriminate between left-and right--hand MI. Ten subjects underwent 12 EEG-MI-BCI sessions. Two frequency bands, three FC methods, four graph parameters and six electrode sites were evaluated, using statistical and classification analyses. The & beta; band produced the largest number of statistically significantly discriminating and most stable features for the majority of subjects, and also the best classification features, suggesting that engagement of needed brain regions may be more important for stability and distinguishability among MI tasks than inhibition of unneeded cortical regions. The Cz electrode stood out in terms of largest number of statistically significantly discriminating features. The motif synchroni-zation (MS) method produced the largest number of significantly discriminating features, the most stable, most discriminating features and best classification features for most subjects. Since this method ignores amplitude changes, this seems to indicate that signal variation patterns are more important for feature stability and class separability. Eigenvector centrality (EC) was the most stable graph parameter for most subjects while both EC and strength (S) were the most discriminating. In summary, using features from the MS method, & beta; band, EC and/ or S parameters, and central electrodes (Cz), result in the best combination for the task of distinguishing left from right-hand MI.

BIOMEDICAL SIGNAL PROCESSING AND CONTROL 85, 105061, 2023. DOI: 10.1016/j.bspc.2023.105061

[P142-2023] "Review: using rolled-up tubes for strain-tuning the optical properties of quantum emitters"

Gomes, G.*; Gomes, M. L. F.*; Silva, S. F. C. da; **Garcia Jr.***, A.; Rastelli, A.; **Couto Jr., O. D. D.***; Malachias, A.; **Deneke, C.***

Rolled-up tubes based on released III-V heterostructures have been extensively studied and established as optical resonators in the last two decades. In this review, we discuss how light emitters (quantum wells and quantum dots) are influenced by the inherently asymmetric strain state of these tubes. Therefore, we briefly review whispering gallery mode resonators built from rolled-up III-V heterostructures. The curvature and its influence over the diameter of the rolled--up micro- and nanotubes are discussed, with emphasis on the different possible strain states that can be produced.

Experimental techniques that access structural parameters are essential to obtain a complete and correct image of the strain state for the emitters inside the tube wall. In order to unambiguously extract such strain state, we discuss x-ray diffraction results in these systems, providing a much clearer scenario compared to a sole tube diameter analysis, which provides only a first indication of the lattice relaxation in a given tube. Further, the influence of the overall strain lattice state on the band structure is examined via numerical calculations. Finally, experimental results for the wavelength shift of emissions due to the tube strain state are presented and compared with theoretical calculations available in literature, showing that the possibility to use rolled-up tubes to permanently strain engineer the optical properties of build--in emitters is a consistent method to induce the appearance of electronic states unachievable by direct growth methods.

NANOTECHNOLOGY 34[41], 412001, 2023. DOI: 10.1088/1361-6528/ace4d1

[P143-2023] "Search for electroweak production of charginos and neutralinos at N/s=13 TeV in final states containing hadronic decays of WW, WZ, or WH and missing transverse momentum"

Tumasyan, A.; Adam, W.; **Chinellato, J. A.***; et al. CMS Collaboration

This Letter presents a search for direct production of charginos and neutralinos via electroweak interactions. The results are based on data from proton-proton collisions at a center--of-mass energy of 13 TeV collected with the CMS detector at the LHC, corresponding to an integrated luminosity of 137 fb-1. The search considers final states with large missing transverse momentum and pairs of hadronically decaying bosons WW, WZ, and WH, where H is the Higgs boson. These bosons are identified using novel algorithms. No significant excess of events is observed relative to the expectations from the standard model. Limits at the 95% confidence level are placed on the cross section for production of mass-degenerate wino-like supersymmetric particles & chi;⠂& PLUSMN; 1 and & chi;⠂02, and mass-degenerate higgsino-like supersymmetric particles & chi;⠂& PLUSMN;1,& chi;⠂02, and & chi;⠂03. In the limit of a nearly-massless lightest supersymmetric particle & chi;⠂01, wino-like particles with masses up to 870 and 960 GeV are excluded in the cases of & chi;⠂02 & RARR; Z & chi;⠂01 and & chi;⠂02 & RARR; H & chi;⠂01, respectively, and higgsino-like particles are excluded between 300 and 650 GeV. & COPY; 2022 The Author(s). Published by Elsevier B.V. This is an open access article under the CC BY license (http://creativecommons .org /licenses /by /4 .0/). Funded by SCOAP3.

PHYSICS LETTERS B 842, 137460, 2023. DOI: 10.1016/j.physletb.2022.137460

[P144-2023] "Semiclassical electron and phonon transport from first principles: application to layered thermoelectrics"

Chaves, A. S.; Pizzochero, M.; Larson, D. T.; **Antonelli, A.***; Kaxiras, E.

Thermoelectrics are a promising class of materials for renewable energy owing to their capability to generate electricity from waste heat, with their performance being governed by a competition between charge and thermal transport. A detailed understanding of energy transport at the nanoscale is thus of paramount importance for developing efficient thermoelectrics. Here, we provide a comprehensive overview of the methodologies adopted for the computational design and optimization of thermoelectric materials from first-principles calculations. First, we introduce density-functional theory, the fundamental tool to describe the electronic and vibrational properties of solids. Next, we review charge and thermal transport in the semiclassical framework of the Boltzmann transport equation, with a particular emphasis on the various scattering mechanisms between phonons, electrons, and impurities. Finally, we illustrate how these approaches can be deployed in determining the figure of merit of tin and germanium selenides, an emerging family of layered thermoelectrics that exhibits a promising figure of merit. Overall, this review article offers practical guidelines to achieve an accurate assessment of the thermoelectric properties of materials by means of computer simulations.

JOURNAL OF COMPUTATIONAL ELECTRONICS DOI: 10.1007/s10825-023-02062-4 Primeira data de acesso: JUN 2023

[P145-2023] "Silicon anisotropy in a bi-dimensional optomechanical cavity"

Kersul, C. M.*; Benevides, R.; **Moraes, F.*; Aguiar, G. H. M. de*;** Wallucks, A.; Groblacher, S.; **Wiederhecker, G. S.*; Alegre, T. M. P.***

In this work, we study the effects of mechanical anisotropy in a 2D optomechanical crystal geometry. We fabricate and measure devices with different orientations, showing the dependence of the mechanical spectrum and the optomechanical coupling on the relative angle of the device to the crystallography directions of silicon. Our results show that the device orientation strongly affects its mechanical band structure, which makes the devices more susceptible to orientation fabrication imperfections. Finally, we show that our device is compatible with cryogenic measurements, reaching a ground state occupancy of 0.25 phonons at mK temperature.

APL PHOTONICS 8[5], 056112, 2023. DOI: 10.1063/5.0135407

[P146-2023] "SN1987A neutrino burst: limits on flavor conversion"

Dedin Neto, P.*; Santos, M. V. dos*; Holanda, P. C. de*; Kemp, E.*

In this paper, we revisit the SN1987A neutrino data to see its constraints on flavor conversion. We are motivated by the fact that most works that analyze this data consider a specific conversion mechanism, such as the MSW (Mikheyev--Smirnov-Wolfenstein) effect, although flavor conversion is still an open question in supernovae due to the presence of neutrino-neutrino interactions. In our analysis, instead of considering a specific conversion mechanism, we let the electron antineutrino survival probability P-(ee) over bar be a free parameter. We fit the data from Kamiokande-II, Baksan, and IMB detected spectrum with two classes of models: time-integrated and time-dependent. For the time-integrated model, it is not possible to put limits above 1s (68% confidence level) on the survival probability. The same happens for the time-dependent model when cooling is the only mechanism of antineutrino emission. However, for models considering an accretion phase, P-(ee) over bar similar to 0 is strongly rejected, showing a preference for the existence of an accretion component in the detected antineutrino flux, and a preference for normal mass ordering when only the MSW is present.

EUROPEAN PHYSICAL JOURNAL C 83[6], 459, 2023. DOI: 10.1140/epjc/s10052-023-11597-6

[P147-2023] "Stimulated Brillouin scattering by surface acoustic waves in lithium niobate waveguides"

Rodrigues, C. C.*; Zurita, R. O.*; Alegre, T. P. M.*; Wiederhecker, G. S.*

We numerically demonstrate that lithium niobate on insulator (LNOI) waveguides may support confined short -wavelength surface acoustic waves that interact strongly with optical fields through backward-stimulated Brillouin scattering in both Z- and X-cut orientation. We conduct fully anisotropic simulations that consider not only mov-ing boundary and photoelastic forces, but also roto-optic forces for the Brillouin interaction. Our results indicate that photoelasticity dominates the Brillouin gain and can reach as high as GB/Qm = 0.43 W-1m-1 in standard ridge waveguides.

JOURNAL OF THE OPTICAL SOCIETY OF AMERICA B-OPTICAL PHYSICS 40[5], D56-D63, 2023. DOI: 10.1364/JOSAB.482656

[P148-2023] "Switching field distribution of ultradense arrays of single-crystalline magnetic nanowires"

Pierrot, A.; Yi, D.; Peres, L.; Soulantica, K.; Cours, R.; Warot-Fonrose, B.; Marcelot, C.; Respaud, M.; **Beron, F.***; Blon, T.

Ultradense arrays of magnetic nanoelements present considerable interest for extending areal densities in magnetic recording media, provided that they display high switching fields and corresponding low standard deviations. Here, we report the switching field distribution of bottom-up synthesized single-crystalline vertical Co nanowires self-organized in 2D hexagonal superlattices. The combined shape and Co hexagonal compact magnetocrystalline anisotropies in individual nanowires of diameter as small as 6 nm define a robust perpendicular magnetic anisotropy despite important interactions in superlattices of 10 x 10(12) NWs/in(2). Using quantitative analysis of temperature-dependent first-order reversal curves, we capture the switching field distribution in this dipolar-coupled perpendicularly magnetized nanomagnets. First, the interwire dipolar interactions are treated separately and show a dominant mean field character with temperature independent amplitudes that scale with the nanowire packing fraction. Then, the intrinsic switching field distribution, namely, independent of interwire interactions, is determined as a function of temperature in the 5-300 K range. The mean value and deviation are both found to be driven by the intrawire dipolar interaction and the temperature-dependent uniaxial magnetocrystalline anisotropy, but of smaller amplitudes than those expected from bulk behavior. With coercive fields ranging between 0.3 and 0.8 T, the switching field deviations relative to coercivity reach 20%, which is a moderate value regarding pitch arrays as small as 8 nm.

APPLIED PHYSICS LETTERS 122[26], 2023 DOI: 10.1063/5.0148774

[P149-2023] "Symmetry breaking in core-valence double ionisation of allene"

Idebohn, V.; Linguerri, R.; **Cornetta, L. M.*;** Olsson, E.; Wallner, M.; Squibb, R. J.; Couto, R. C.; Karlsson, L.; Nyman, G.; Hochlaf, M.; Eland, J. H. D.; Agren, H.; Feifel, R.

Allene serves as a model to study multiple ionization of organic molecules. Here, the authors use synchrotron radiation-based multi-particle coincidence techniques and high-level ab initio calculations to propose a simple physical model to elucidate the symmetry breaking in core-valence double ionization of allene. Conventional electron spectroscopy is an established one-electron-at-the-time method for revealing the electronic structure and dynamics of either valence or inner shell ionized systems. By combining an electron-electron coincidence technique with the use of soft X-radiation we have measured a double ionisation spectrum of the allene molecule in which one electron is removed from a C1s core orbital and one from a valence orbital, well beyond Siegbahns Electron-Spectroscopy-for-Chemical--Analysis method. This core-valence double ionisation spectrum shows the effect of symmetry breaking in an extraordinary way, when the core electron is ejected from one of the two outer carbon atoms. To explain the spectrum we present a new theoretical approach combining the benefits of a full self-consistent field approach with those of perturbation methods and multi-configurational techniques, thus establishing a powerful tool to reveal molecular orbital symmetry breaking on such an organic molecule, going beyond Lowdins standard definition of electron correlation.

COMMUNICATIONS CHEMISTRY 6[1], 137, 2023. DOI: 10.1038/s42004-023-00934-1

[P150-2023] "Synchronization of silicon thermal free-carrier oscillators"

Luiz, G. de O.*; Rodrigues, C. C.*; Alegre, T. P. M.*; Wiederhecker, G. S.*

Recent exploration of collective phenomena in oscillator arrays has highlighted the potential to access a range of physical phenomena, from fundamental quantum many-body dynamics to the solution of practical optimization problems using photonic Ising machines. Spontaneous oscillations often arise in these oscillator arrays as an imbalance between gain and loss. Due to coupling between individual arrays, the spontaneous oscillation is constrained and leads to interesting collective behavior, such as synchronized oscillations in optomechanical oscillator arrays, ferromagnetic-like coupling in delay-coupled optical parametric oscillators, and binary phase states in coupled laser arrays. A key aspect of arrays is not only the coupling between the individuals but also their compliance toward neighbor stimuli. One self-sustaining photonic oscillator that can be readily implemented in a scalable foundry based technology is based on the interaction of free carriers, temperature, and the optical field of a resonant silicon photonic microcavity. Here, we demonstrate that these silicon thermal free-carrier (FC) oscillators are extremely compliant to external excitation and can be synchronized up to their 16th harmonic using a weak seed. Exploring this unprecedented compliance to external stimuli, we also demonstrate robust synchronization between two thermal FC oscillators.

JOURNAL OF THE OPTICAL SOCIETY OF AMERICA B-OPTICAL PHYSICS 40[7], 1779-1785, 2023. DOI: 10.1364/JOSAB.482609

[P151-2023] "The CARNAUBA X-ray nanospectroscopy beamline at the Sirius-LNLS synchrotron light source: Developments, commissioning, and first science at the TARUMA station"

Tolentino, H. C. N.; Geraldes, R. R.; **Silva, F. M. C. da***; Guaita, M. G. D.; Camarda, C. M.; Szostak, R.; Neckel, I. T.; Teixeira, V. C.; Hesterberg, D.; Perez, C. A.; Galante, D.; Callefo, F.; Neto, A. C. P.; Kofukuda, L. M.; Sotero, A. P. S.; Moreno, G. B. Z. L.; Luiz, S. A. L.; Bueno, C. S. N. C.; Lena, F. R.; Westfahl, H.

We review the main developments and first commissioning experiments at the CARNAUBA X-ray nanoprobe beamline, recently installed at the brand-new Sirius 4th-generation synchrotron radiation source at the Brazilian Synchrotron Light Laboratory (LNLS). The paper briefly discusses the X-ray nanoprobe instrument, emphasizing the first deployed experimental station TARUMA, and showcases preliminary results in a broad range of areas that benefit from diverse sample environments. Research domains like photovoltaics, photonics, electrocatalysis, geoscience, and agriculture are investigated from the viewpoint of chemistry, atomic structure, morphology, and redox dynamics phenomena covered by the beamline techniques.

Finally, future capabilities are presented based on a new instrument under development.

JOURNAL OF ELECTRON SPECTROSCOPY AND RELATED PHENOMENA 266, 147340, 2023. DOI: 10.1016/j.elspec.2023.147340

[P152-2023] "Third-harmonic generation in silica wedge resonators"

Soares, J. H.*; Santos, L. F. dos*; Santos, F. G. S.*; Inga, M.*; Espinel, Y. A. V.*; Wiederhecker, G. S.*; Alegre, T. P. M.*

Whispering-gallery-mode microcavities are known to have a high optical quality factor, making them suitable for nonlinear optical interactions. Here, third-harmonic generation is observed using a relatively small radius wedge silicon oxide optical microcavity. The small radii wedge microdisks can be dispersion-tailored to obtain either normal or anomalous group velocity dispersion. In our case, we operated in the normal dispersion regime preventing frequency comb generation by suppressing IR cascading four-wave mixing. This approach allowed for a clean third-harmonic generation at phase-matched visible optical modes. Tunability of the third-harmonic emis-sion was obtained due to a combination of thermo-optical and Kerr effects. An additional thermal control of the phase-matching condition allows the optimization of the third-harmonic generation, and an agreement between this process and the couple-modetheory was demonstrated. & COPY; 2023 Optica Publishing Group

JOURNAL OF THE OPTICAL SOCIETY OF AMERICA B-OPTICAL PHYSICS 40[6], 1407-1412, 2023. DOI: 10.1364/JOSAB.482611

[P153-2023] "Using ZrNb and ZrMo oxide nanoparticles as catalytic activity boosters supported on Printex L6 carbon for H2O2 production"

Trevelin, L. C.; Valim, R. B.; Lourenco, J. C.; **Siervo, A. de***; Rocha, R. S.; Lanza, M. R. V.

Oxygen reduction reaction (ORR) is an important reaction which is widely applied in advanced oxidative processes (AOP) through the in-situ electrogeneration of hydrogen peroxide. Oxygen gas can either be reduced to hydrogen peroxide via two-electron pathway or be converted to water in a competitive way via four-electron pathway. In this study, we report the effective enhancement of H2O2 generation in K2SO4 0.1 mol/L (pH 2) through the application of Printex L6 carbon (PL6C) modified with zirco-nium/niobium (ZrNb) and zirconium/molybdenum (ZrMo) oxides compared to unmodified PL6C. The proposed catalysts were prepared by the polymeric precursors synthesis method (on carbon). The cata-lysts were analyzed by X-ray fluorescence (FRX), transmission electron microscopy (TEM), and X-ray pho-toelectron spectroscopy (XPS), and were electrochemically characterised by cyclic voltammetry (CV) and hydrodynamic linear sweep voltammetry (LSV). The electroactivity of ZrNb/PL6C and ZrMo/PL6C oxides was analyzed in the ratio of 50/50 w/w. The results obtained from the electrochemical characterisations of the electrodes showed that the application of 5% ZrNb/PL6C and 1% ZrMo/PL6C yielded H2O2 selectivity of 84.3 and 77%, respectively, compared to 84.3% recorded for the unmodified PL6C. Also, based on the application of a determined current density, 5% ZrNb/PL6C and 1% ZrMo/PL6C recorded a potential shift of 200 and 400 mV to less negative potentials, respectively, compared to the unmodified PL6C, which implies in less energy consumption. The results obtained from the morphological and surface character-isations of the materials pointed to a practically homogeneous distribution of ZrO2, Nb2O5, and MoO3 with particle size of ca. 5 nm on the PL6C surface compared to the unmodified PL6C which exhibited par-ticle size of ca. 30-50 nm.

ADVANCED POWDER TECHNOLOGY 34[9], 104108, 2023. DOI: 10.1016/j.apt.2023.104108

***Autores da comunidade IFGW**
Fonte: Web of Science on-line (WOS)

Defesas de Dissertações do IFGW

[D011-2023] "Microfabricação de Guias de Onda e Cavidades Ópticas em Anel em Filmes Finos de Niobato de Lítio"
Aluno: Felipe Boechat Mazzi
Orientador: Prof. Dr. Felippe Alexandre Silva Barbosa
Data: 03/08/2023

[D012-2023] "Certificação de estados emaranhados locais"
Aluno: Gabriela Ruiz
Orientador: Prof. Dr. Rafael Luiz da Silva Rabelo
Data: 04/08/2023

[D013-2023] "Síntese e caracterização elétrica de filmes LbL de poli(etilenaimina) a e poli(ácido acrílico) e seus compósitos com óxido de grafeno reduzido"
Aluno: Shirley Monteiro Vieira da Rocha Hossack
Orientador: Prof. Dr. Varlei Rodrigues
Data: 10/08/2023

[D014-2023] "Avaliação de modelos de mama voxelizados para dosimetria em mamografia"
Aluno: Giovanna Tramontin Carneiro
Orientador: Profa. Dra. Alessandra Tomal
Data: 14/08/2023

[D015-2023] "Influência de tensionamento e ressonâncias óticas de emissores em tubos enrolados formados por InAlGaAs/GaAs"
Aluno: Gabriel Gomes dos Santos
Orientador: Prof. Dr. Christoph Deneke
Data: 16/08/2023

[D016-2023] "Simulação de magnetorecepção aviária em computadores quânticos"
Aluno: Pedro Henrique Pereira de Carvalho Alvarez
Orientador: Prof. Dr. Marcos Cesar de Oliveira
Data: 21/08/2023

[D017-2023] "Anéis de vorticidade em colisões relativísticas de íons pesados"
Aluno: Vítor Hugo Ribeiro
Orientador: Prof. Dr. Jun Takahashi
Data: 24/08/2023

Defesas de Teses do IFGW

[T009-2023] "Aspectos de Simulações Atomísticas: Processos e Sistemas Fora do Equilíbrio"
Aluno: Vitor Fidalgo Cândido
Orientador: Prof. Dr. Maurice de Koning
Data: 25/08/2023

[T010-2023] "Procura por fontes pontuais de nêutons em dados do observatório Pierre Auger"
Aluno: Danelise de Oliveira Franco
Orientador: Profa. Dra. Carola Dobrigkeit Chinellato
Data: 28/08/2023

Fonte: Portal IFGW/Pós-graduação - Agenda de Colóquios, Defesas e Seminários.
Disponível em: http://portal.ifi.unicamp.br/pos-graduacao

Defesas de Dissertações e Teses do PECIM

[P002-2023] "Diálogos possíveis entre a História das Ciências e a interdisciplinaridade no Ensino de Ciências: o caso da fabricação de soda na Europa dos séculos XVIII e XIX"
Aluno: Ivo Bernardi de Freitas
Orientador: Prof. Dr. Gildo Girotto Júnior
Banca: Prof. Dr. Gildo Girotto Júnior - IQ/ UNICAMP, Profa. Dra. Silvia Fernanda de Mendonça Figueirôa - IG/ UNICAMP, Prof. Dr. Mauricio Compiani - IG/ UNICAMP, Dr. Ivã Gurgel - Instituto de Física, Universidade de São Paulo /São Paulo, Dr. José Otavio Baldinato - Instituto Federal de São Paulo / Salto, Profa. Dra. Ana de Medeiros Arnt - IB/ UNICAMP (suplente), Dr. Alexandre Bagdonas - Universidade Federal de Lavras /Lavras (suplente), Dra. Tathiane Milaré - Universidade Federal de São Carlos - campus Araras /Araras (suplente), **Prof. Dr. Mauricio Urban Kleinke* - IFGW/ UNICAMP** (suplente)
Data: 21/08/2023
Exame de Defesa: Doutorado

Fonte: Página do Programa de Pós-Graduação Multiunidades em Ensino de Ciências e Matemática - PECIM
Disponível em: https://www.pecim.unicamp.br/bancas

Abstracta

Instituto de Física
Diretor: Profa. Dra. Mônica Alonso Cotta
Diretora Associada: Prof. Dr. Marcos Cesar de Oliveira
Universidade Estadual de Campinas - UNICAMP
Cidade Universitária Zeferino Vaz
13083-859 - Campinas - SP - Brasil
e-mail: secdir@ifi.unicamp.br
Fone: +55 19 3521-5300

Publicação

Biblioteca do Instituto de Física Gleb Wataghin
http://portal.ifi.unicamp.br/biblioteca
Instagram: @bif.unicamp

Diretora Técnica: Sandra Maria Carlos Cartaxo
Coordenadora da Comissão de Biblioteca: Profa. Dra. Arlene Cristina Aguilar

Elaboração:
Maria Graciele Trevisan (Bibliotecária)
contato: infobif@ifi.unicamp.br